Turkish Journal of Earth Sciences

Volume 30
Number 8 *SI-1*

Article 2

1-1-2021

GPS derived finite source mechanism of the 30 October 2020 Samos earthquake, Mw =6.9, in the Aegean extensional region

BAHADIR AKTUĞ

İBRAHİM TİRYAKİOĞLU

HASAN SÖZBİLİR

HALUK ÖZENER

ÇAĞLAR ÖZKAYMAK

See next page for additional authors

Follow this and additional works at: https://journals.tubitak.gov.tr/earth

 Part of the Earth Sciences Commons

Recommended Citation

AKTUĞ, BAHADIR; TİRYAKİOĞLU, İBRAHİM; SÖZBİLİR, HASAN; ÖZENER, HALUK; ÖZKAYMAK, ÇAĞLAR; YİĞİT, CEMAL ÖZER; SOLAK, HALİL İBRAHİM; EYÜBAGİL, EDA ESMA; GELİN, BENGİSU; TATAR, ORHAN; and SOFTA, MUSTAFA (2021) "GPS derived finite source mechanism of the 30 October 2020 Samos earthquake, Mw =6.9, in the Aegean extensional region," *Turkish Journal of Earth Sciences*: Vol. 30: No. 8, Article 2. https://doi.org/10.3906/yer-2101-18
Available at: https://journals.tubitak.gov.tr/earth/vol30/iss8/2

This Article is brought to you for free and open access by TÜBİTAK Academic Journals. It has been accepted for inclusion in Turkish Journal of Earth Sciences by an authorized editor of TÜBİTAK Academic Journals. For more information, please contact academic.publications@tubitak.gov.tr.

GPS derived finite source mechanism of the 30 October 2020 Samos earthquake, Mw =6.9, in the Aegean extensional region

Authors
BAHADIR AKTUĞ, İBRAHİM TİRYAKİOĞLU, HASAN SÖZBİLİR, HALUK ÖZENER, ÇAĞLAR ÖZKAYMAK, CEMAL ÖZER YİĞİT, HALİL İBRAHİM SOLAK, EDA ESMA EYÜBAGİL, BENGİSU GELİN, ORHAN TATAR, and MUSTAFA SOFTA

This article is available in Turkish Journal of Earth Sciences: https://journals.tubitak.gov.tr/earth/vol30/iss8/2

TÜBİTAK

Turkish Journal of Earth Sciences

http://journals.tubitak.gov.tr/earth/

Research Article

Turkish J Earth Sci
(2021) 30: 718-737
© TÜBİTAK
doi:10.3906/yer-2101-18

GPS derived finite source mechanism of the 30 October 2020 Samos earthquake, Mw = 6.9, in the Aegean extensional region

Bahadır AKTUĞ[1], İbrahim TİRYAKİOĞLU[2,3,*], Hasan SÖZBİLİR[4,5], Haluk ÖZENER[6], Çağlar ÖZKAYMAK[3,7], Cemal Özer YİĞİT[8], Halil İbrahim SOLAK[9], Eda Esma EYÜBAGİL[2], Bengisu GELİN[6], Orhan TATAR[10], Mustafa SOFTA[4]

[1]Department of Geophysical Engineering, Ankara University, Ankara, Turkey
[2]Department of Geomatics Engineering, Engineering Faculty, Afyon Kocatepe University, Afyonkarahisar, Turkey
[3]Earthquake Implementation and Research Center of Afyon Kocatepe University, Afyonkarahisar, Turkey
[4]Department of Geological Engineering, Engineering Faculty, Dokuz Eylül University, İzmir, Turkey
[5]Earthquake Research and Application Center of Dokuz Eylül University, İzmir, Turkey
[6]Department of Geodesy, Kandilli Observatory and Earthquake Research Institute, Boğaziçi University, İstanbul, Turkey
[7]Department of Geological Engineering, Engineering Faculty, Afyon Kocatepe University, Afyonkarahisar, Turkey
[8]Faculty of Engineering, Department of Geomatics Engineering, Gebze Technical University, Gebze-Kocaeli, Turkey
[9]Distance Education Vocational School, Afyon Kocatepe University, Afyonkarahisar, Turkey
[10]Faculty of Engineering, Department of Geological Engineering, Cumhuriyet University, Sivas, Turkey

Received: 23.01.2021 • **Accepted/Published Online:** 07.05.2021 • **Final Version:** 30.10.2021

Abstract: A submarine area close to the Turkish and Greek border between the cities of Samos-Greece and Seferihisar-Turkey has been shaked on October 30, 2020 by a Mw= 6.9 earthquake. In this study, the finite source mechanism of the Samos earthquake was investigated using geodetic methods and the coseismic behavior of the earthquake was modeled. The observed coseismic displacements at 62 sites were inverted for the fault geometry and the slips. The mainshock did not generate an on-land surface rupture. However, the uniform slip modeling shows a finite source of 43.1 km long and 16 km wide rupture, which slips 1.42 m along a north dipping normal fault extending from the Aegean Sea floor to a depth down to ~13 km. While the uniform slip model is consistent with the seismological solutions and provides a sufficient fit to the far field coseismic offsets, a distributed slip model is necessary to account for the near field coseismic displacements.

Key words: Samos, Global Positioning System (GPS), coseismic, earthquake, slip, rupture process

1. Introduction

The coastal areas of the Aegean Sea have been experienced a number of earthquakes since ancient times; most of them resulted in destructive damages on human being. The faults that caused these destructive earthquakes survive both under the Aegean Sea and on the Anatolian and Greek lands in an extensional back-arc tectonic setting (Figure 1). One of these faults, the Samos Fault, which is an east-west striking and north dipping normal fault forming the northern margin of the Samos island, was documented by several seismogenic centers as seismogenic source of the Samos earthquake with a magnitude of 6.9 earthquake struck on Friday, 30 October 2020, about 13 km in the Aegean Sea between Sığacık Gulf of Turkish coast and the Greek island of Samos. More than five thousand buildings were damaged 17 of which are completely collapsed as a result of the earthquake; 117 people are known to have died in Bayraklı district of İzmir city, 70 km far from the epicentral area, with more than one thousand injured. As of December 26, over 5000 aftershocks have been recorded (Sözbilir et al. 2020).

The region is dominated by earthquake swarm after the mainshock occurred on the 30th of October 2020 (Mw = 6.9), which is located at the central-eastern part of the Aegean microplates, an extremely deformed extensional back-arc area. Fault plane geometry that manifests itself under the Aegean Sea with the intensity of aftershocks has shown that the seismic source that caused the Samos earthquake was under the sea. Generate Mapping Tools (GMT) software was used to visualize all data (Wessel et al., 2019).

* Correspondence: itiryakioglu@aku.edu.tr

This work is licensed under a Creative Commons Attribution 4.0 International License.

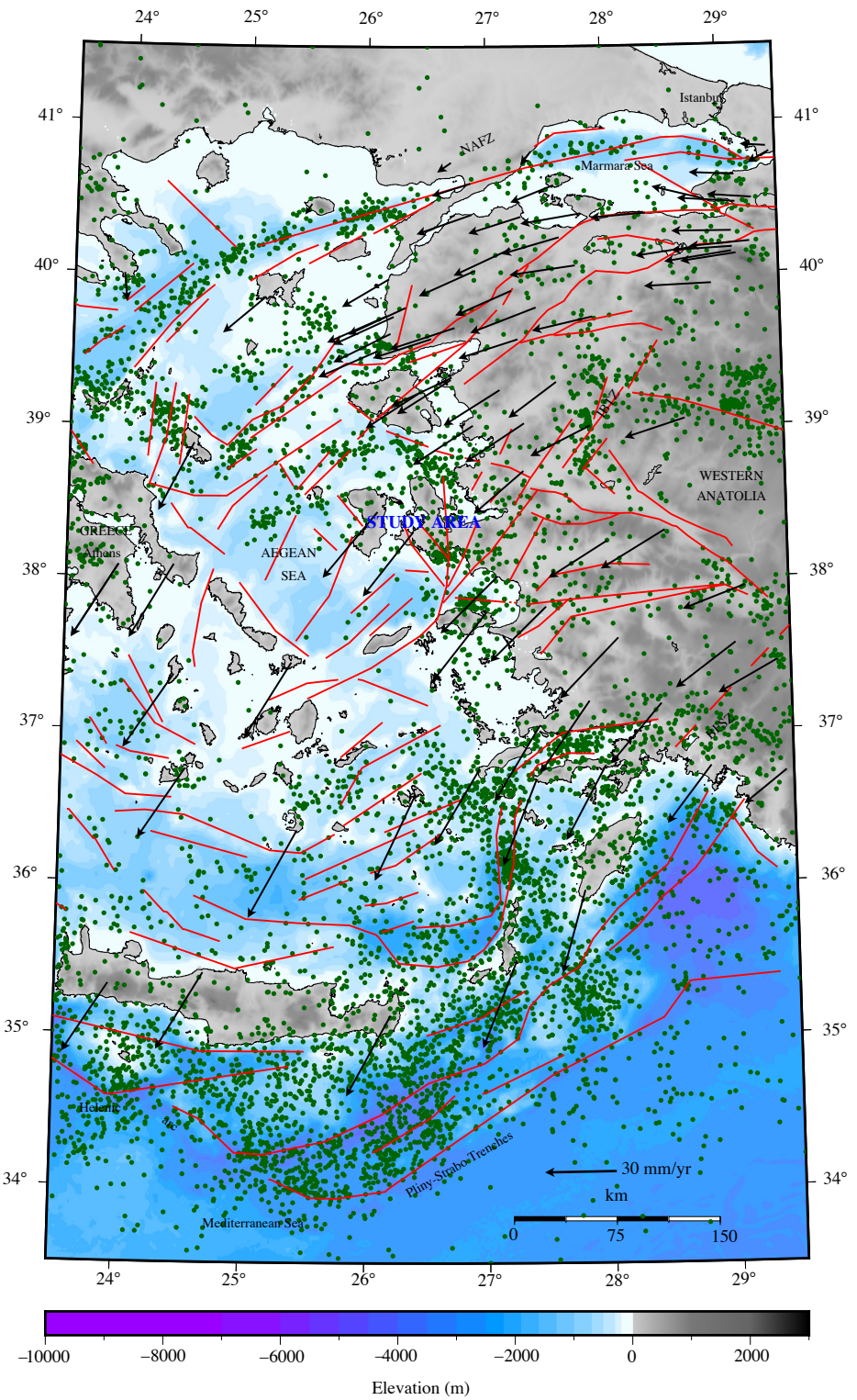


Figure 1. Major active tectonic structures between Greece and western Anatolia. Bathymetry extracted from the CGMW/UNESCO Morpho-Bathymetry of the Mediterranean Sea (Brossolo et al., 2012). Faults are compiled from Mascle and Martin, 1990; Papanikolaou et al., 2002; Pavlides et al., 2009; Yaltırak, 2002; Ocakoğlu et al., 2004; Yaltırak et al., 2012; Chatzipetros et al., 2013; Özkaymak et al., 2013; Sboras et al., 2011; Elitez and Yaltırak, 2014; Tur et al., 2015; Sözbilir et al., 2008, 2009, 2011, 2017; Emre et al., 2018; Eytemiz and Erdeniz, 2020. Abbreviations: NAFZ: North Anatolian Fault Zone; İBTZ: İzmir-Balıkesir Transfer Zone; BFSZ: Burdur-Fethiye Shear Zone. Black arrows represent velocities taken from Aktuğ et al., (2009) and Reilinger et al., (2006).

2. Seismo-tectonic setting

The Samos earthquake occurred in eastern part of the Aegean Sea, a back-arc basin behind the Hellenic subduction zone (McKenzie, 1978). The Aegean Sea and surrounding, is seismically one of the most active and rapidly extending region on the Earth, have been deformed under the control of a N–S extensional tectonic regime at a rate reaching up to 30/40 mm/yr since the Pliocene (Dewey and Şengör, 1979; Jackson and Mckenzie, 1984; Le Pichon et al., 1995; Aktuğ et al., 2009; Eyübagil et al., 2020). Crustal extension is accommodated by a combination of normal-slip and strike-slip motions along active faults, especially in central Aegean and western Anatolia (Mascle and Martin, 1990; Taymaz et al., 1991; Tan et al., 2014). In terms of strain, the amount of crustal extension between Samos and western Anatolia (the broader Izmir area) is 7.4 mm/yr according to Vernant et al., (2014) based on GNSS (Global Navigation Satellite System) data modeling.

The interaction with the Mediterranean oceanic plate underlying the Aegean microplate, and westward motion of the Anatolian microplate along the North Anatolian Fault and East Anatolian Fault results in progressively deformation pattern in these regions (e.g., Papazachos and Comninakis, 1971; McKenzie 1972, 1978; McClusky et al., 2000). The westward motion of the Anatolian microplate is transferred by a noncomplex interaction to the Aegean extensional area, which includes the western and southern region of Turkish coasts and its vicinity of Aegean Islands. In the literature, many of researcher had worked these interactions to evaluate current deformation pattern and seismic activity of the region. From these researchers, Tan et al. (2014) investigated a detailed micro seismicity and fault plane solutions that are used to determine the current tectonic activity of the prominent zone of seismicity near Samos Island and Kuşadası Bay. They stated that the geometry of each segment is quite simple and indicates planar dislocations gently dipping with an average dip of 40–45°, maintaining a constant dip through the entire seismogenic layer down to 15 km depth. In addition to that, fault plane solutions evaluated from both P-wave polarity data and moment tensor analysis with magnitude of up to Mw :4.9 in 2008-2012 show the predominance of normal faulting, along with strong contribution of the strike slip motion, with a N-S trending extension (Tan et al., 2014). After the 30 October 2020 Samos earthquake, other seismotectonic studies were carried out focusing on the fault model, the tsunami, the deformation field, and aftershocks that were the source of the earthquake in and around the island of Samos were evaluated (Çetin et al; 2020/2; Ganas et al., 2020; Papadimitrou et al., 2020; Akıncı et al., 2021; Doğan et al., 2021; Elias et al., 2021; Evelpidou et al., 2021).

Historical and moderate to high instrumental earthquakes ranging from BC 200 to AD 1893 in this region are documented by several researchers (Figure 2a), (Guidoboni et al.,1994; Taxeidis, 2003; Ambraseys, 2009; Stucchi et al., 2013; Tan et al., 2014; ISC, 2020).

According to historical catalogues, 200 BC earthquake was significantly harmed the people of Samos Island. In addition to that, the Roman province of Asia suffered from devastating earthquake in 47 AD. Samos, Cibyra, Smyrna, Ephesus, Laodicea, and Hierapolis were damaged by this earthquake. They stated that the epicenter of the 47 AD earthquake was in Samos Island and intensity of the quake was VII (Guidoboni et al.,1994; Tan et al., 2008; Ambraseys, 2009). The 1751 AD earthquake is reported to have caused considerable damage to Samos Island and the Turkish coast opposite (Guidoboni et al., 1994; Papazachos and Papazachou, 1997). Besides these earthquakes, there was an earthquake in 1865 AD and 1890 AD that strongly affected Samos Island and Ephesus (Pınar and Lahn, 1952; Ergin et al., 1967; Soysal et al., 1981; Guidoboni et al., 2005; Ambraseys, 2009).

In addition to these significant historical earthquakes, there are many instrumental earthquakes that were affected the region since 1901. These instrumental data indicate a broader zone and shallow-intermediate earthquakes, and there were more than 26000 earthquakes having a magnitude greater than 2, more than 7000 earthquakes having a magnitude greater than 3, and more than 600 earthquakes having a magnitude greater than 4. (Figure 2b, ISC, 2020).

From these earthquakes, the earthquake occurred in1904 with Mw = 6.8 caused a severe damage to the towns and villages along the northwestern coastal area (Tan et al., 2014). Moreover, they stated that while the 20 June 2009 Samos earthquake swarm concentrated near the Pythagorion fault (Chazitrepetros et al., 2013), with an event of Mw: 5.1 with more than 80 events with ML > 1.5 within first 10 days, a second earthquake cluster was observed close to the northeastern coast of the Island near Vathy fault. In addition to that, the largest earthquake was widely felt in Samos and the neighbor islands as well as across the coastal area of western Turkey. The instrumental earthquakes (Mw > 4) occurred in the coastal of Western Anatolia and Samos Island between 1979 and 2020 were compiled and given in Table 1.

30 October 2020 Samos earthquake (Mw = 6.9) occurred at 11:51 (UTC), and ruptured a fault section along the sea, 12 km north of Samos Island (Figure 3). Mainshock focal mechanism solutions of the earthquake given in Table 2. The nearest settlement is 13 km away from the coast of Turkey were severely shaken and damage occurred at several level.

Seismic sources of these earthquakes that have occurred in the instrumental and historic period can be found under the Aegean Sea and on land as NE-SW and

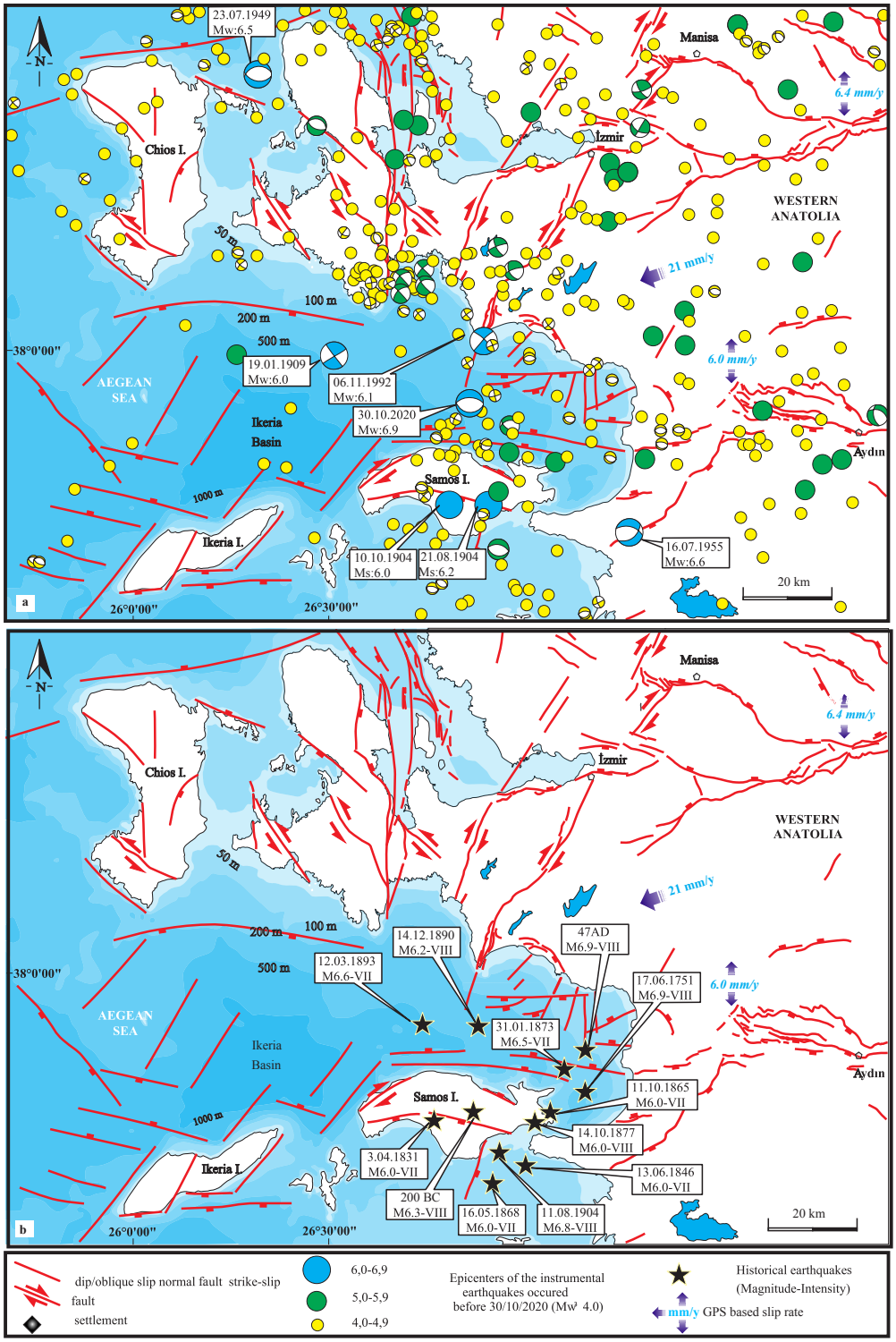


Figure 2. (a). Seismotectonic map of the Eastern part of Aegean Sea region, showing the epicenters of instrumental earthquakes, GPS based slip rate and active faults that responsible for both instrumental and historic earthquakes in the region (b). Distribution on the historical earthquakes that occurred in Samos Island and its vicinity. While the instrumental seismicity between 1900-2020 are compiled from ISC, (2020), information for the historical earthquakes from Taxeidis (2003), Ambraseys (2009) and Stucchi et al. (2013). Active faults which are depicted with red in Turkey are taken from Emre et al. (2018). Other faults in Samos island and vicinity are compiled from Lykousis et al. (1995), Ocakoğlu et al., (2004), Chamot-Rooke and DOTMED working group, (2005), Pavlides et al., (2009), Chazitrepetros et al., (2013), Caputo and Pavlides (2013).

Table 1. The list of instrumental earthquakes (Mw > 4.0) occurred the coastal of Western Anatolia and Samos Island (Latitude range: 37.289° to 38.490° -Longitude range: from 26.156° to 28.639°). The earthquakes are compiled from ISC (2020).

No	Date	Time (UTC)	Latitude (°)	Longitude (°)		Magnitude (Mw)	D (km)
1	14.06.1979	11:44:45	38.7459	26.5832	5.8	11.5	
2	16.06.1979	18:42:01	38.6983	26.5974	5.3	13.0	
3	6.11.1992	19:08:11	38.1311	27.0114	6.1	14.9	
4	2.04.1996	07:59:26	37.8138	26.8666	5.4	14.0	
5	1.03.2001	13:31:19	37.8706	26.7864	4.4	13.0	
6	10.04.2003	00:40:17	38.2424	26.8837	5.8	12.6	
7	17.04.2003	22:34:28	38.2223	27.0248	5.2	16.1	
8	29.01.2005	18:52:29	38.0873	26.8328	4.8	8.8	
9	23.06.2005	22:44:17	37.7214	26.7713	4.6	9.2	
10	17.10.2005	05:45:19	38.1220	26.6440	5.5	11.9	
11	17.10.2005	08:28:53	38.1622	26.6789	4.7	1.8	
12	17.10.2005	09:46:57	38.1806	26.7046	5.8	12.0	
13	17.10.2005	09:55:32	38.1711	26.6924	5.1	15.9	
14	19.10.2005	10:11:31	38.1303	26.6465	4.6	7.7	
15	20.10.2005	21:40:04	38.1261	26.7502	5.9	10.9	
16	29.10.2005	14:48:40	38.0818	26.6729	4.2	0.8	
17	31.10.2005	05:26:41	38.1530	26.6645	4.9	14.1	
18	20.06.2009	08:28:20	37.6473	26.8771	5.1	8.7	
19	26.03.2010	18:35:55	38.2054	26.2652	4.6	16	
20	11.11.2010	20:08:02	37.8756	27.3784	4.6	12.7	
21	27.12.2011	05:59:19	37.9709	27.1835	4.3	8.4	
22	27.01.2012	17:43:20	37.4543	27.1126	4.2	10.2	
23	20.02.2012	06:34:29	38.1483	27.4514	4.4	8.5	
24	21.02.2013	10:18:51	37.3694	26.9293	4.5	7.0	
25	1.05.2014	14:16:12	38.0246	27.0368	4.1	9.6	
26	18.07.2014	03:58:58	38.2407	26.6152	4.0	14.1	
27	11.10.2014	06:42:10	38.2097	27.0548	4.0	11.7	
28	21.10.2014	03:03:57	38.1657	27.1406	4.1	15.7	
29	10.01.2015	04:32:09	38.2036	27.0583	4.3	11.7	
30	27.03.2015	01:42:41	37.9736	27.2293	4.1	7.0	
31	6.07.2015	01:03:48	38.2338	26.5700	4.1	16.8	
32	17.10.2016	01:30:31	37.9376	26.9942	4.3	15.3	
33	8.05.2017	08:47:19	37.8786	27.1437	4.2	10.3	
34	12.05.2017	05:55:45	37.8599	27.1428	4.2	11.4	
35	25.12.2017	05:13:51	38.5779	26.7566	4.9	13	
36	26.07.2018	08:17:52	37.6776	26.7115	4.5	13.2	
37	26 .7.2018	08:17:52	37.6776	26.7115	4.5	13.2	

Table 1. (Continued).

38	28.10.2018	08:15:35	38.2008	26.8557	4.1	14.5	
39	8.08.2019	08:39:07	38.0488	26.8526	4.7	0	
40	30.08.2019	15:38:14	37.4855	26.8329	4.7	10	
41	30.08.2019	17:21:04	37.5207	26.8245	4.5	6.2	
42	16.07.2020	18:09:24	38.3797	26.6830	4.3	0	
43	30.10.2020	11:51:26	37.8442	26.8310	7.0	18.7	
44	30.10.2020	15:14:55	37.8705	26.8358	5.2	0	
45	31.10.2020	05:31:32	37.7600	26.8500	5.0	10	
46	1.11.2020	07:33:07	37.7494	26.8919	4.5	0	

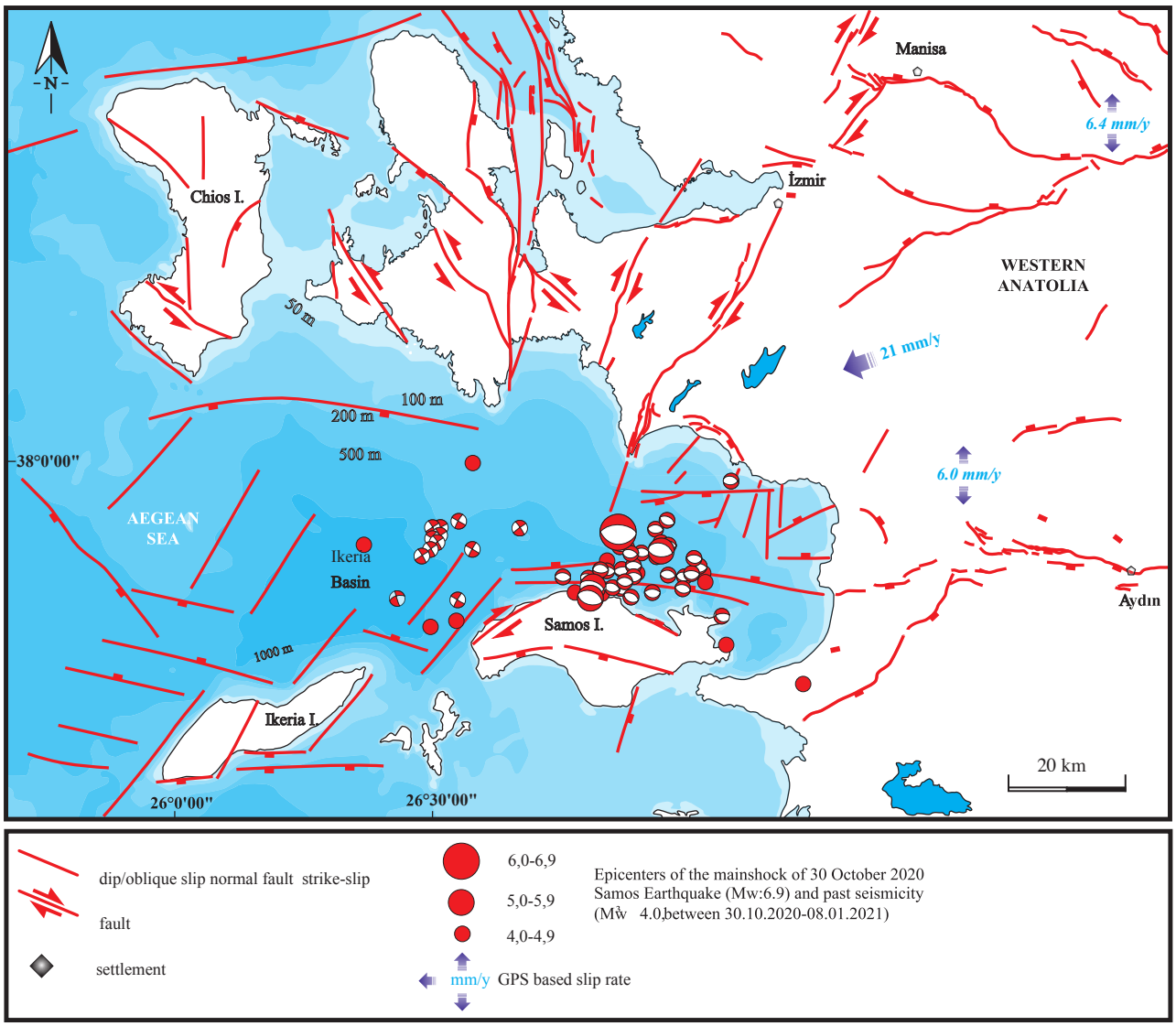


Figure 3. Seismotectonic map of the Eastern part of Aegean Sea region, showing the epicenters of focal mechanism the main shock of 30 October 2020 and aftershocks. Faults are compiled from Lykousis et al., (1995), Ocakoğlu et al., (2004), Chamot-Rooke and DOTMED working group, (2005), Pavlides et al., (2009), Chazitrepetros et al., (2013), Emre et al., (2018), Caputo and Pavlides (2013).

Table 2. Focal mechanism solutions for the mainshock of the 30/10/2020 Samos earthquake (Mw = 6.9) from various seismology centers and GPS (this study).

Nodal Plane 1						Nodal Plane 2				
Model	Long.	Lat.	Strike	Dip	Rake	Strike	Dip	Rake	Depth	Mo
	(°)	(°)	(°)	(°)	(°)	(°)	(°)	(°)	(km)	(dyn × cm)
This Study GPS)	26.901	37.809	288	46	–84	-	-	-	12	2.96×10^{19}
USGS	26.790	37.900	93	61	–91	276	29	–88	11.5	40.87×10^{26}
KOERI	26.790	37.900	97	34	–85	272	55	–93	10	3.00×10^{26}
NOA	26.810	37.900	294	54	–65	76	43	–120	6	26.46×10^{26}
GFZ	26.820	37.900	97	41	–85	272	48	–93	15	3.500×10^{26}
AFAD	26.780	37.890	95	43	–87	270	46	–91	16.5	32.64×10^{26}
IPGP	26.800	37.900	260	36	–116	111	58	–72	14	37.60×10^{26}

Abbreviations: USGS: United States Geological Survey, KOERI: Kandilli Observatory and Earthquake Research Institute, NOA: National Observatory of Athens, GFZ: German Research Centre for Geosciences, AFAD: Disaster and Emergency Management Presidency, IPGP: Institute De Physics Du Globe De Paris. The latitude and longitude is given as the midpoint of the computed rectangular fault. The coordinates are the western endpoint of the finite source.

NW-SE strike slip faults and E-W trending normal faults have produced destructive earthquakes in a way that triggers each other (Figure 3).

3. Geodetic networks data and modelling

3.1. Geodetic networks processing and coseismic displacements

GNSS provides useful information to understand the faulting processes using slip rate of the interseismic, preseismic, coseismic, and postseismic deformation. (Lisowski, 1997; Reilinger et al., 2006; Reddy and Sunil, 2008; Reilinger et al., 2010; Tiryakioglu, 2015,2018a,2018b). In this study, coseismic deformation has been investigated based on GPS observations. 62 GNSS sites covering the region were used (Aktuğ and Kılıçoğlu 2006; Aktuğ et. al., 2009; Özener et al., 2013; Çırmık et al., 2017a; Ganas et al., 2020; Eyübagil et al., 2021; Havazlı and Özener 2021; https://drive.google.com/file/d/1bjSCZu2WnukJeHWLfcNpZtuxYtARLfeh/). These GNSS sites include CORS-TR (Continuously Operating Reference Stations, Turkey), TNFGN (the Turkish National Fundamental GNSS Network), NOA (National Observatory of Athens), and GNSS sites/points established from previous researchers and authors of this study. Eight GNSS stations (ANDR, CHIO, IKAR, KALY, MKYN, NAXO, LESV, SAMO) belonging NOA were on islands located around the earthquake epicenter. The RINEX (Receiver Independent Exchange Format) data of the sites in previous studies were provided via project managers and authors of these studies. The most recent GNSS observations from TNFGN sites before the earthquake and GNSS observations from CORS-TR stations during, before, and after the earthquake were obtained from authorized institutions. The combined GNSS network consists of 62 sites in total 29 of which are campaign types and 33 of which are CORS stations. GNSS sites are at distances ranging from 10 to160 km with a northern density.

Min. 8-h with 30s interval GNSS measurement was carried out between 5th and 8th of November 2020 at campaign type sites to calculate post-earthquake coordinates Figure 4).

GAMIT/GLOBK software was used for the evaluation of GNSS data. 29 IGS stations with stable time series were used for stabilization and IGS final option for orbit information; earth rotations parameters and antenna information were selected to obtain more accurate coordinates. Moreover, the antenna phase center was derived according to the height-dependent model. During the analysis, LC (L3), which is the ionosphere-independent linear combination of the L1 and L2 carrier waves, and the FES2004 Ocean Tide Loading (OTL) grid was used (Gülal et al., 2013; Herring et al., 2015; Tiryakioğlu et al., 2013, 2015, 2017a, 2017b, 2018b, 2019). As a result, daily adjusted coordinates in ITRF2014 frame of all sites were calculated with the accuracy of ~6 mm for the horizontal components. In order to calculate the displacement caused by the earthquake at GNSS sites, the differences between the coordinates of the sites before and after the earthquake were used. Since the last coordinates of the campaign type sites were before the year 2020, the coordinates of these sites have been moved to the pre-earthquake epoch (2020.10). In determining pre-earthquake epoch for each



Figure 4. GPS observations (pillar-DMRC Site, Ground monument -GMDR Site).

site, ITRF2014 velocity calculated using GAMIT/GLOBK was used (Figure 5). The observed surface displacements for all GNSS sites used in this study are given in Table 3.

Coseismic displacement are tightly correlated with the time series models. Short term and long-term solution for the displacement are clearly exposed using continuous GPS data (Aktuğ et al., 2010; Tiryakioğlu et al., 2017a, 2017b, 2019). The observed coseismic displacements in short term solutions of IZMI and MNTS stations are given in Figure 6.

Significant displacements have been observed in particular for the stations near the epicenter, which are indicated in bold in Table 3. As can be seen from the detected coseismic displacement in Table 3, the North components of these stations had more coseismic displacement than the East component. The coseismic displacements in the North component lie in the range of –12 (KALY) and –372 (SAMO) mm, with uncertainties of 2–9 mm (negative values shows south direction). Significant displacements in the East component lie in the range from 9.0 to 65.3 mm, with uncertainties of 2–9 mm. From the results, we found that the maximum coseismic displacement of –372 mm in the North components occurred at station SAMO, the closest site to the earthquake epicenter with a distance of 10 km. Stations SIGA and HZUR had the maximum coseismic displacement values in Turkish side and the coseismic displacement of 132.6 mm, 23.3 mm and 136.6 mm, 65.3 mm at the north and east components, respectively. Furthermore, no significant coseismic displacement was observed in the remaining stations (28 sites).

3.2 Fault geometry inversion

Using the finite dislocation equations in an elastic half-space Okada (1985), the observed surface displacements were inverted for the fault geometry and slip vector. The relation between the coseismic surface offsets and the

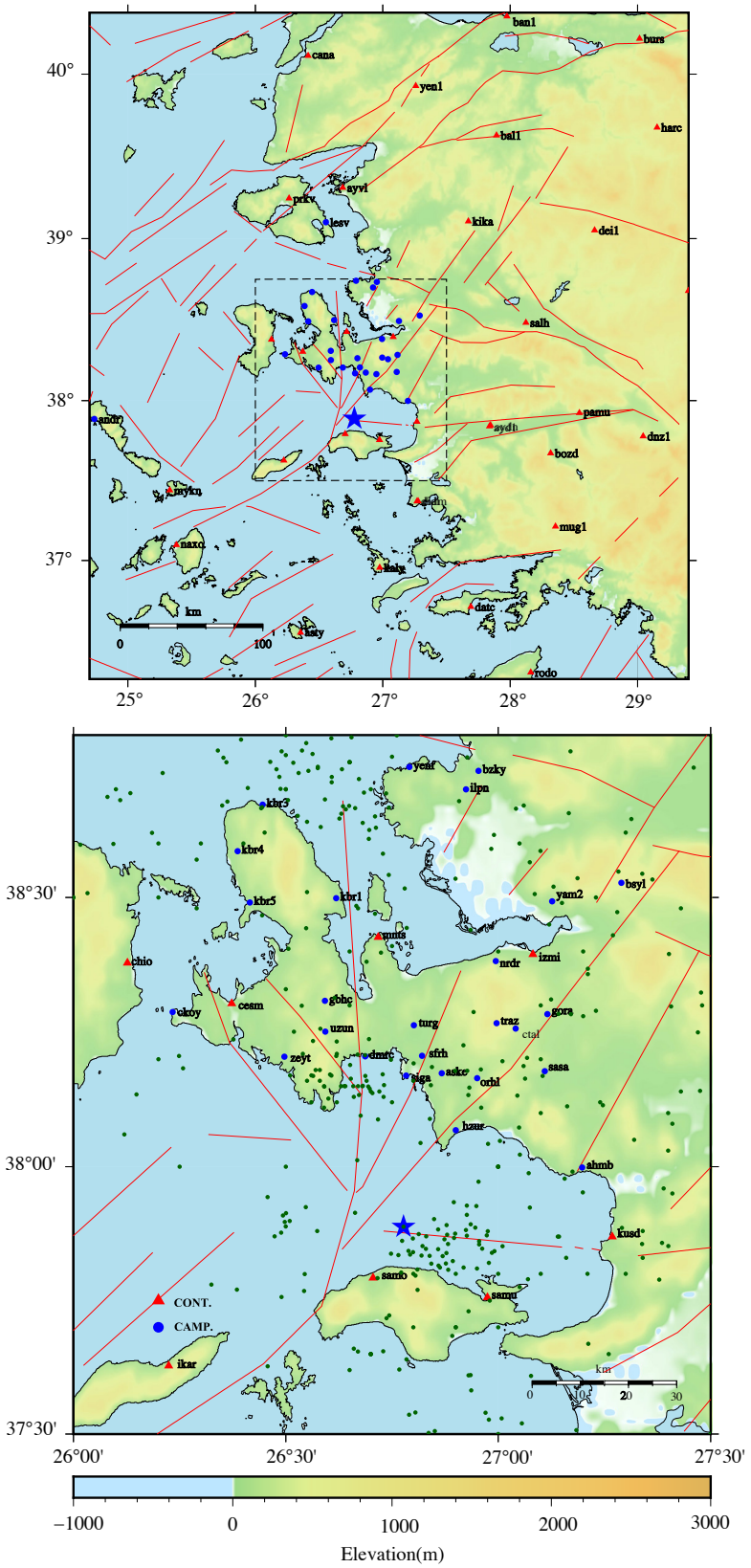


Figure 5. GPS network and aftershocks between the earthquakes with Mw = 2.0 and Mw = 5.0 (Green Circles 31.10.2020–31.12.2020). Red triangles and blue circles represent continuous stations and campaign sites, respectively.

Table 3. Observed surface displacements and standard errors at GPS sites.

Site	Λ	φ	Δe	Δn	$\sigma_{\Delta e}$	$\sigma_{\Delta n}$
	(°)	(°)	(mm)	(mm)	(mm)	(mm)
AHMB	27.197	37.9984	**15.4**	**29**	4.5	5.3
ANDR	24.736	37.886	1.0	3.0	3.7	3.7
ASKE	26.867	38.174	**36.8**	**100.6**	3.5	4.6
ASTY	26.355	36.545	–1.0	–6.0	3.7	3.8
AYD1	27.837	37.840	–1.0	2.0	3.0	3.0
AYDN	27.846	37.846	2.0	–5.0	4.7	5.0
AYVL	26.686	39.311	0.0	6.0	2.8	3.0
BAL1	27.892	39.629	0.0	2.0	2.8	3.0
BAN1	27.974	40.348	–1.0	4.0	2.8	3.1
BOZD	28.317	37.672	0.0	–4.0	4.9	5.1
BSYL	27.289	38.527	–4.3	**28.3**	3.1	3.8
BURS	29.015	40.214	–1.0	1.0	2.8	3.0
BZKY	26.953	38.734	4.8	6.1	4.1	4.7
CANA	26.414	40.111	–2.0	2.0	2.8	3.0
CESM	26.372	38.303	**–13.0**	**51.0**	2.8	3.0
CHİO	26.126	38.378	**–9.0**	**19.0**	2.8	3.0
CKOY	26.233	38.287	**–20.1**	13.0	3.8	4.4
CTAL	27.041	38.257	**26.5**	**57.4**	4.5	5.4
DATC	27.691	36.708	–1.0	0.0	3.0	3.2
DEI1	28.662	39.050	0.0	0.0	2.8	3.0
DIDI	27.268	37.371	–1.0	–8.0	2.8	3.0
DIDM	27.277	37.373	4.0	**–18**	4.7	5.0
DMRC	26.686	38.205	**16.3**	**130.8**	3.7	4.0
DNZ1	29.043	37.778	0.0	6.0	2.8	3.0
GBHC	26.592	38.308	0.6	**76.8**	4.6	5.2
GORA	27.115	38.283	**32.1**	**38.7**	3.2	3.6
HARC	29.152	39.677	–1.0	1.0	2.8	3.0
HZUR	26.900	38.068	**65.3**	**136.6**	4.7	3.8
IZMI	27.081	38.394	**13.0**	**34.0**	2.8	3.0
IKAR	26.224	37.628	**–12.0**	**-28.0**	3.3	3.4
ILPN	26.924	38.699	–1.2	**26.4**	3.9	5.0
KALY	26.976	36.955	4.0	**–12.0**	3.0	3.3
KBR1	26.618	38.498	2.4	**36.2**	3.0	3.6
KBR3	26.445	38.671	–2.2	**25.2**	4.8	4.2
KBR4	26.386	38.585	1.5	**46.4**	5.4	5.1
KBR5	26.415	38.490	**–45.1**	**28.5**	5.9	6.2
KIKA	27.671	39.105	3.0	5.0	3.0	3.0
KUSD	27.268	37.869	–7.0	–2.0	4.5	4.6
LESV	26.553	39.100	–1.0	8.0	3.2	3.3
MNTS	26.717	38.426	6.0	**47.0**	3.2	3.2

Table 3. (Continued).

MUG1	28.355	37.214	–3.0	0.0	2.8	3.0
MYKN	25.328	37.441	0.0	–2.0	3.1	3.1
NAXO	25.381	37.098	–2.0	–2.0	2.8	2.9
NRDR	26.994	38.382	8.0	**46.8**	5.0	5.7
ORHL	26.950	38.164	**40.2**	**86.3**	3.9	5.3
PAMU	28.543	37.923	–1.0	–6.0	4.8	5.1
PRKV	26.264	39.245	0.0	5.0	3.2	3.9
RODO	28.161	36.292	0.0	–1.0	3.3	3.7
SALH	28.123	38.483	1.0	2.0	3.0	3.1
SAMO	26.705	37.792	**–59.0**	**–372.0**	3.7	3.7
SAMU	26.974	37.755	**–8.54**	**–48.92**	0.7	1.1
SASA	27.109	38.177	**22.7**	**43.1**	3.6	4.4
SFRH	26.820	38.206	**19.7**	**97.4**	6.0	6.6
SİGA	26.783	38.169	**23.3**	**132.6**	9.6	10.3
TRAZ	26.996	38.267	**16.8**	**60.1**	4.1	4.8
TURG	26.801	38.263	**22.9**	**80.4**	4.8	5.6
USK1	29.398	38.678	–1.0	–1.0	2.9	3.0
UZUN	26.592	38.251	4.3	**96.4**	5.2	5.3
YAM2	27.126	38.492	3.3	**32.6**	4.3	4.7
YEN1	27.258	39.928	0.0	2.0	2.8	3.0
YENF	26.790	38.741	3.4	8.2	3.7	4.1
ZEYT	26.496	38.204	–7.3	**99.5**	6.0	6.4

**Bold value represents statistically significant coseismic displacement with respect to 3-sigma threshold.*

fault geometry and slip vector was modelled as elasto-static Green's functions. The slip vector consists of only strike-slip and dip-slip components, and no tensile component (opening) was allowed during the inversion. The slip vector is linearly related to the observed surface displacements; whereas, the relation between the surface displacements and fault geometry is non-linear. The objective function which is defined as the weighted residual sum of squares (WRSS) between the observed and the modeled displacements will usually have several local minima. For this reason, a hybrid optimization algorithm which benefits from both the global and local optimization methods scheme was employed. The main benefit of the global optimization is the ability to avoid local minima; whereas, the local optimization methods are more efficient. In a two-step approach, we first inverted the coseismic displacements for the fault geometry with a constant uniform slip over the initial fault geometry. In the second step, the slip vector was estimated by fixing the fault geometry found in the previous step. The details of the employed inversion scheme can be found in (Aktuğ et al., 2010). For the global optimization, the Simulated Annealing was used with a Boltzmann temperature model (Kirkpatrick et al., 1983). While Simulated Annealing is a proven technique to approximate the global minimum, it is not as efficient as local optimization methods such as quasi-Newton methods. Thus, the results were refined using a BFGS (Broyden–Fletcher–Goldfarb–Shanno) algorithm (Fletcher, 1987). The observed and modeled displacements for the uniform slip model are shown in Figure 7.

The inversion of the geodetic coseismic offsets provides an unambiguous finite source solution as opposed to point source mechanisms. The vertical precision of GPS measurements is up to an order of magnitude worse than the horizontal, which is more pronounced in the survey type observations and not necessarily accounted for in the formal uncertainties. To account for this, the vertical components of the observed offsets are down-weighted to one third of the original uncertainties. The distribution of the sites at which the coseismic offsets are obtained has an impact on the independent resolution of the fault geometry and slips. The geometry and slips are estimated in two steps to reduce the possible correlation between the fault geometry and slips. The general trade-off between the fault geometry parameters is given in Figure 8.

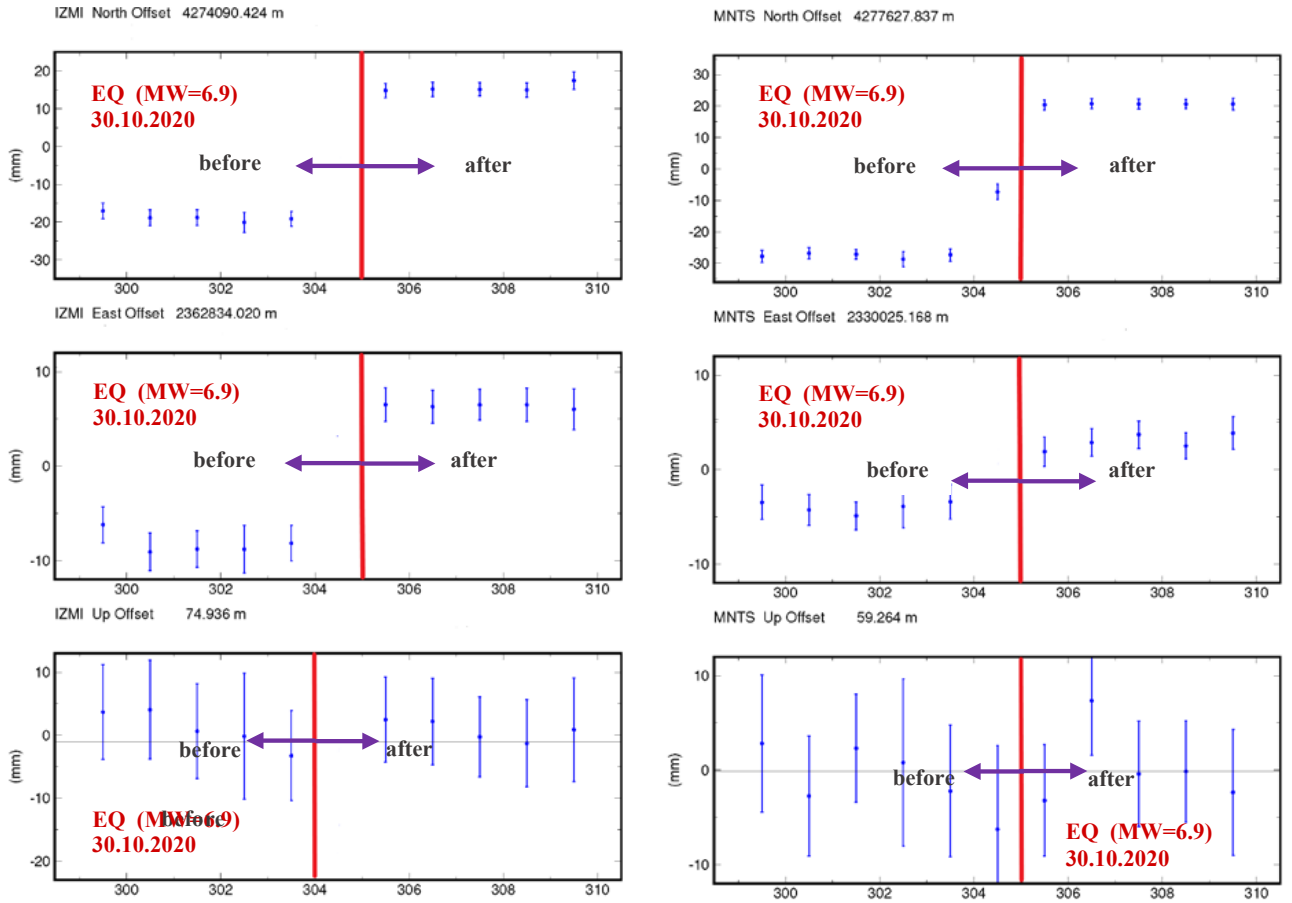


Figure 6. Observed coseismic displacements at IZMI and MNTS sites.

3.3. Distributed slip

The distribution of the slip on the fault plane was estimated using a constrained optimization scheme. The method employs Okada's semi-infinite space model to simulate elastic Green's functions in order to converge to the observed coseismic displacements (Wang et al., 2009). Using the fault geometry determined in the previous step, a distributed slip model was estimated using the steepest descent method. The coseismic offsets at GPS sites were used to invert for the slip patches in a homogenous elastic half-space. A grid of 2.5 × 4 km slip patches defined over a fault plane of 43 km × 30 km was estimated. The distributed slip is shown in Figure 9. The results show that almost all the slip is confined down to a depth of 12.5 km. The slips larger than 1 m are limited down to a depth of 7.5 km. The modelled and observed coseismic offsets at GPS sites are shown in Figure 10. As opposed to the uniform slip model which successfully models the observed offsets at far field sites and fails at two near field sites, the distributed slip approach successfully models at both near and far fields coseismic observations.

4. Discussion and conclusion

In accordance with N-S extensional tectonics of the Aegean Region, the coseismic displacements calculated from the geodetic data also confirm pure N-S extension. The largest movement caused by the 30 October 2020 Samos earthquake (Mw = 6.9) occurred at the SAMO station, which is the closest station with 10 km to the earthquake epicenter, with 372 mm at south component. Similar results were calculated by Çetin et al., (2020/2) and Ganas et al., (2020). In Seferihisar and its vicinity, the maximum coseismic displacement is 136.6 mm at the north component. Significant movements in the region caused by the earthquake are between Ikaria and Kuşadası according to Figure 6. This fact suggests that the stress accumulation caused by this earthquake on the region may be transferred to the north of Samos in addition to the ruptured fault tips where western and eastern extension of Ikaria basin and Büyük Menderes basin, respectively.

The failure occurred on a fault NE-SW trending fault with an estimated strike of 288°, which is consistent with the findings of (Doğan et al., 2021). The coseismic inversion of dense GPS array in this study reveals a finite

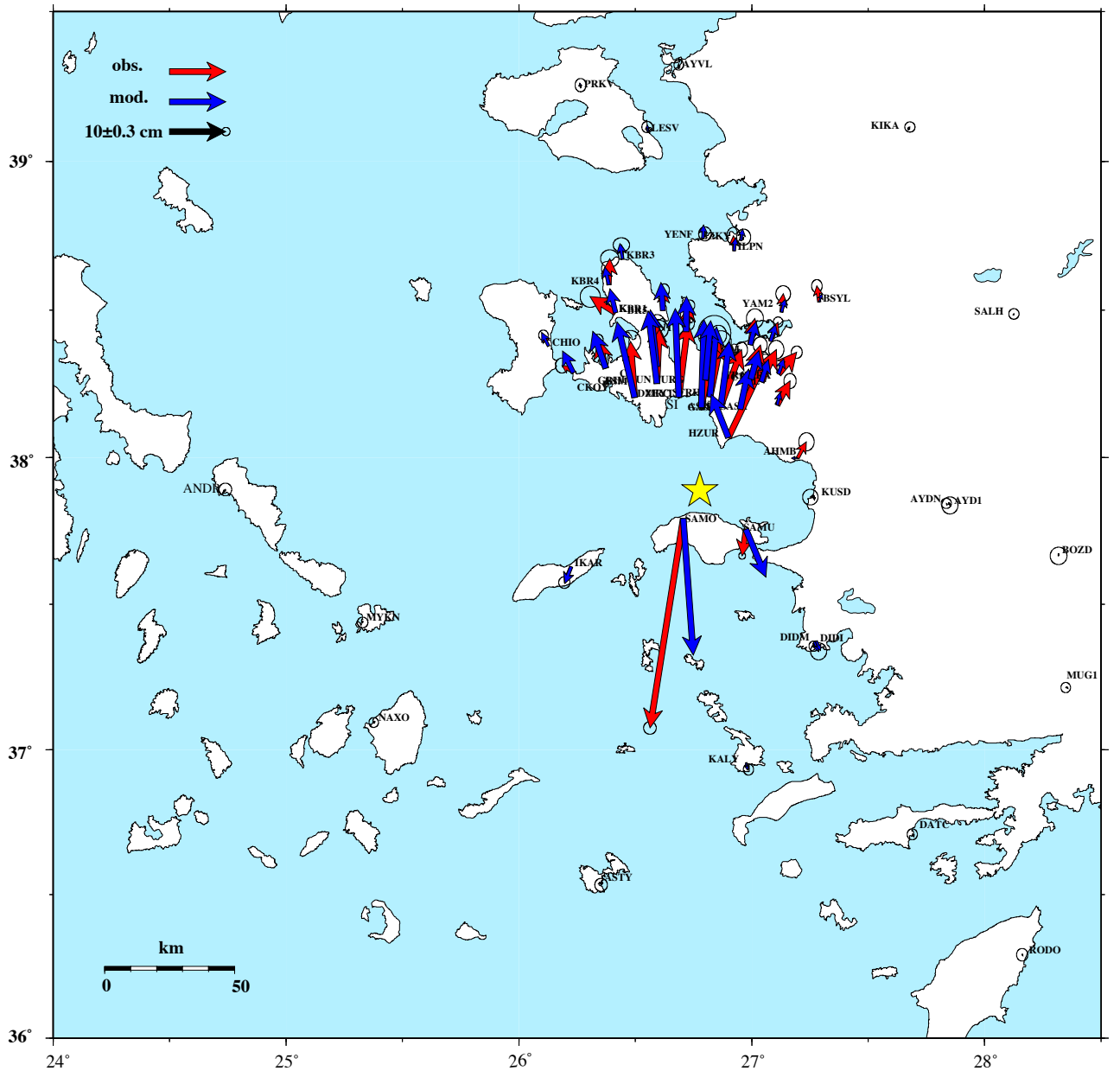


Figure 7. Observed and modeled coseismic displacements for a uniform slip model. Observed and modeled coseismic displacements at GNSS sites are shown in red and blue, respectively. Observed GNSS displacements consists of both continuous and survey-mode observations. Error ellipses are at %95 confidence level.

source of 43.1 km, which is close to 37 km given by (Elias et al., 2021) and about half of 80–100 km given by Doğan et al. (2021). Similarly, estimated width of the fault in uniform slip modeling was 16 km, very close to 17 km found by Elias et al., 2021. However, the average slip of 2.1 m estimated by Elias et al. (2021) appears to be higher than our estimation of 1.42 in uniform slip modeling.

However, Altunel and Pınar (2021) recently published an article and put forward a different kinematic model to describe seismic sources of the Samos earthquake. They stated that the roughly E-W and NNW-SSE trending Ephesus Fault, which controls the southwestern rim of Küçük Menderes Graben (Sümer, 2015), continues further west in the sea to connect with faults in north of Samos Island, there should be a step over to the right via possible a transfer fault somewhere in northeast of the island. However, according to seismic profiles in the Aegean Sea between Samos Island and Kuşadası bay (Lykousis et al., 1995; Chamot-Rooke and DOTMED working group, 2005; Pavlides et al., 2009; Chazitrepetros et al., 2013),

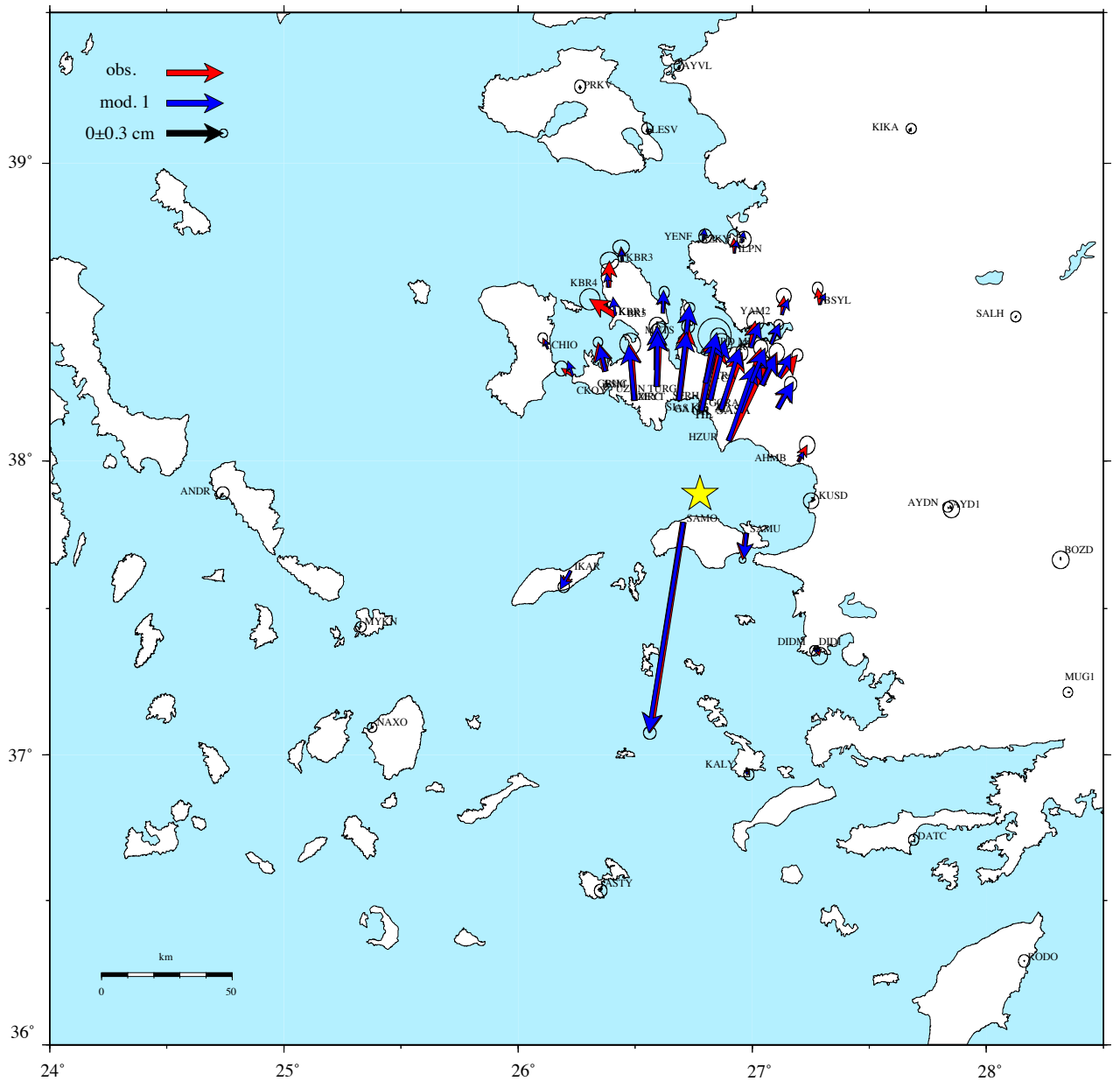


Figure 8. Trade-off matrix for the inverted fault geometry parameters for the uniform-slip model. Best-fit geometry parameter set was inverted for 100 experiments for a constant slip rate of 1 m. Each experiment is represented as a dot in the plots. The strike and dip are in degrees, moment is in 10^{25} dyne-cm, X-coord and Y-coord are the longitude and latitude in degrees, width and depth are in km. The moment is included as an auxiliary parameter since as the slip is fixed, the moment is not an independent parameter but instead a function of length and width.

Samos Fault lies through E-W trending and possibly connecting to the Kuşadası Fault Zone, which includes the active normal faults of Büyük Menderes Graben.

Besides the seismic studies in the nearest Samos region, cosmogenic surface dating-based paleo seismological studies were performed along the Kalafat and Yavansu Faults of Kuşadası Fault Zone, which lies in the eastern part of the Samos Fault. Mozafari et al., (2019) stated that at least three earthquakes rupture identified between 3.6 ka to 15 ka with an estimated long-term slip rate of 1.0 mm/y for Kalafat Fault, between 2.0 ka and 7.9 ka with an estimated long-term slip rate of 0.6 mm/y for Yavansu Fault. According to their results, the recurrence interval did not follow a uniform trend like other active faults in Western Anatolia (e.g., Kürçer et al., 2019). For these reasons, the possibility of triggering of these faults, which have not produced earthquake for a long time, due to the Samos earthquake should be examined.

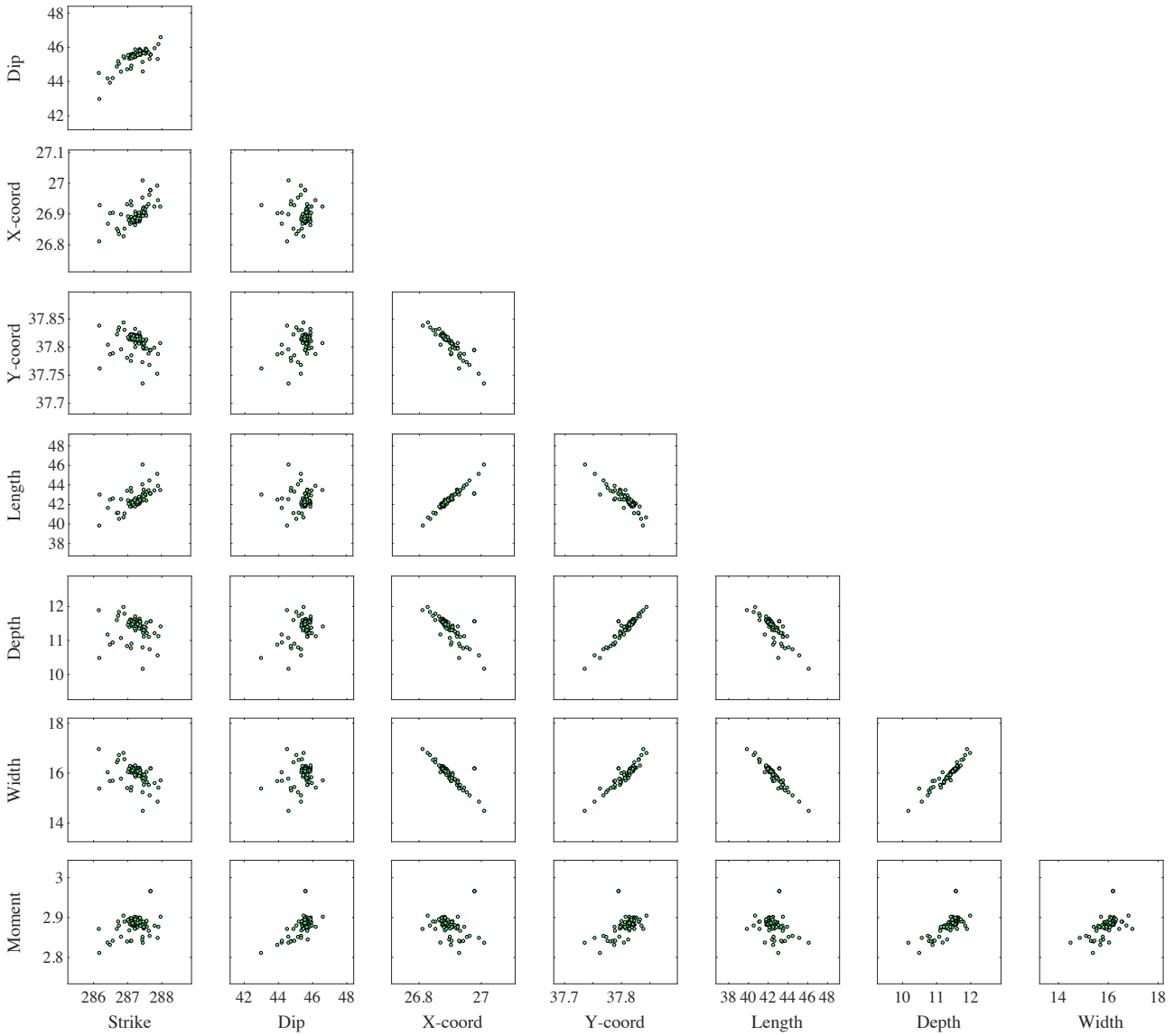


Figure 9. Distributed coseismic slip on the resolved geometry of Samos Fault.

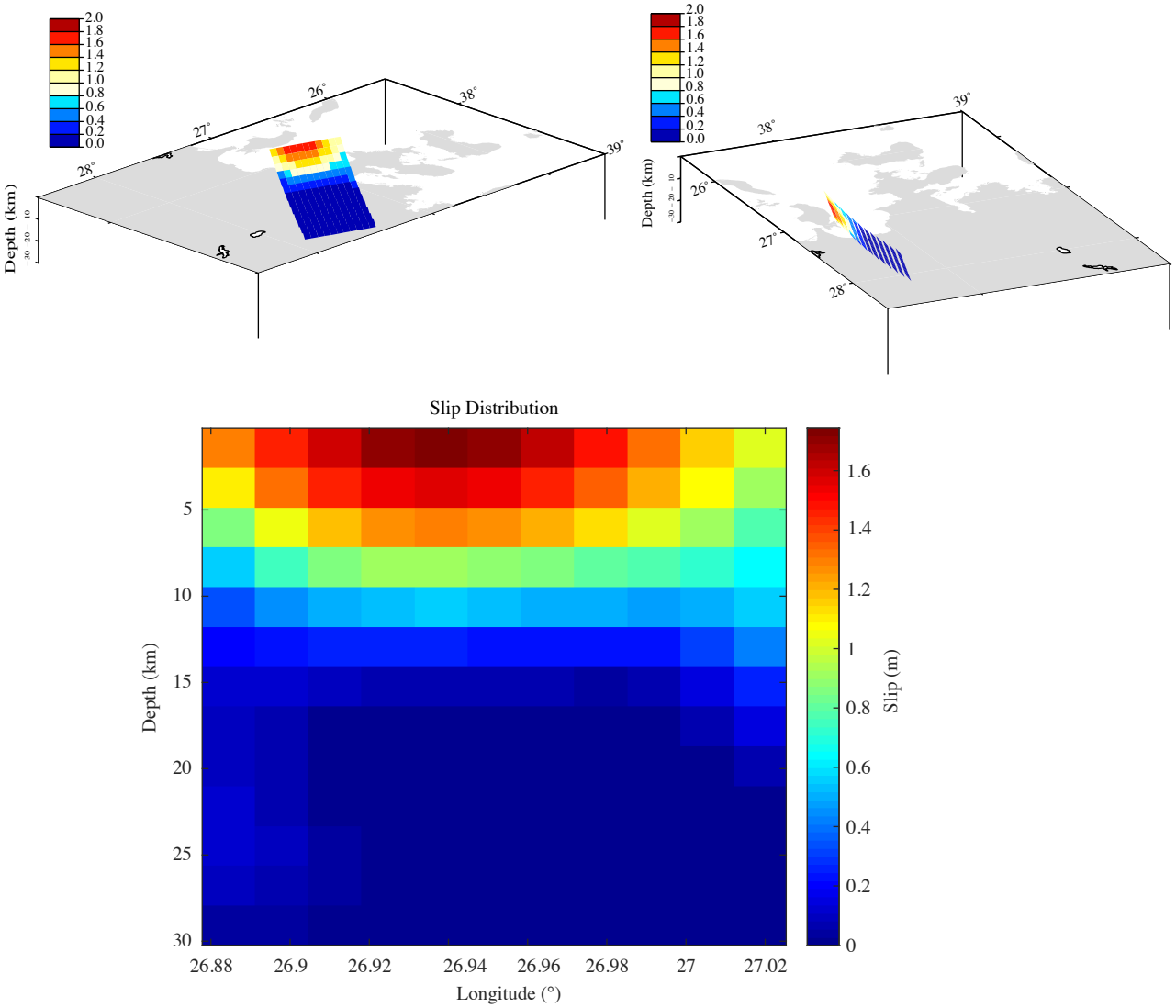


Figure 10. Observed and modeled coseismic displacements for a distributed slip model. Observed and modeled coseismic displacements at GNSS sites are shown in red and blue, respectively. Observed GNSS displacements consists of both continuous and survey-mode observations. Error ellipses are at %95 confidence level.

Acknowledgment

This research was supported by Afyon Kocatepe University Research Foundation (project number: AKÜ-BAP 19. FENBİL.2-19. FENBİL.11), The Scientific and Technological Research Council of Turkey (TÜBİTAK) with the project numbered (5200101), TÜBITAK-ÇAYDAG under grant No: 108Y295 and Boğaziçi University Scientific Research Projects (BAP) under grant No: 6359. We would like to thank TÜBİTAK for the rapid financial support they provided to the field study immediately after the earthquake. We would like to particularly acknowledge the TUSAGA-Active GNSS Network and the private Greek network, Smartnet Greece for GNSS data. The authors are grateful to numerous graduate students of Geomatics Engineering Department of Afyon Kocatepe University, General Directorate of Mapping and other institutions for their support of the GNSS measurements and data.

References

Akıncı A, Cheloni D, Dindar AA (2021). The 30 October 2020 Samos (Eastern Aegean Sea) Earthquake: effects of source rupture, path and local-site conditions on the observed and simulated ground motions. 12 February 2021, PREPRINT (Version 1) available at Research Square doi: 10.21203/rs.3.rs-215817/v1

Aktuğ B, Kılıçoğlu A (2006). Recent crustal deformation of İzmir, Western Anatolia and surrounding regions as deduced from repeated GPS measurements and strain field. Journal of Geodynamics 41 (5): 471-484. doi: 0.1016/j.jog.2006.01.004

Aktuğ B, Nocquet JM, Cingöz A, Parsons B, Erkan Y et al. (2009). Deformation of Western Turkey from a combination of permanent and campaign GPS data: limits to block-like behavior. Journal of Geophysical Research 114 (5): 1978-2012. doi: 10.1029/2008JB006000

Aktuğ B, Kaypak B, Çelik RN (2010). Source parameters for the Mw= 6.6, 03 February 2002, Çay Earthquake (Turkey) and aftershocks from GPS, Southwestern Turkey. Journal of Seismology 14(3):445-456. doi: 10.1007/s10950-009-9174-y

Altunel E, Pinar A (2021). Tectonic implications of the Mw 6.8, 30 October 2020 Kuşadası Gulf earthquake in the frame of active faults of Western Turkey. Turkish Journal of Earth Sciences 30: 436-448.

Ambraseys N (2009). Earthquakes in the Mediterranean and Middle East: a multidisciplinary study of seismicity up to 1900. New York, NY, USA: Cambridge University Press.

Brosolo L, Mascle J, Loubrieu B (2012). Morphobathymetric Map of the Mediterranean Sea. Paris, France: publication CCGM/CGMW, UNESCO.

Caputo R. and Pavlides S (2013): The Greek Database of seismogenic sources (GreDaSS), version 2.0.0: A compilation of potential seismogenic sources (Mw > 5.5) in the Aegean Region. http://gredass.unife.it/, doi: 10.15160/unife/gredass/0200

Çetin KÖ, Mylonakis G, Sextos A, Stewart JP (2020/02). Hellenic Association of Earthquake Engineering: Report 2020/02 Earthquake Engineering Association of Turkey Earthquake Foundation of Turkey Earthquake Engineering Research Institute (USA)Geotechnical Extreme Events Reconnaissance Association: Report GEER-069 doi: 10.18118/G6H088

Chamot-Rooke N, Dotmed Working Group (2005). DOTMED – Deep offshore tectonics of the Mediterranean: A synthesis of deep marine data in eastern Mediterranean. Mémoire de la Société géologique de France & American Association of Petroleum Geologists 177: 64.

Chatzipetros A, Kiratzi A, Sboras S, Zouros N, Pavlides S (2013). Active faulting in the north-eastern Aegean Sea Islands. Tectonophysics 597: 106-122. doi: 10.1016/j.tecto.2012.11.026

Çırmık A, Pamukçu O, Gönenç T, Kahveci M, Şalk M et al. (2017a). Examination of the kinematic structures in İzmir (Western Anatolia) with repeated GPS observations (2009, 2010 and 2011). Journal of African Earth Sciences 126: 1-12. doi: 10.1016/j.jafrearsci.2016.11.020

Dewey JF, Şengör AMC (1979). Aegean and surrounding regions: Complex multiplate and continuum tectonics in a convergent zone. Geological Society of America Bulletin 90 (1): 84-92. doi: 10.1130/0016-7606(1979)90<84:AASRCM>2.0.CO;2

Doğan G G, Yalçıner A C, Yüksel Y, Ulutaş E, Polat O et al. (2021). The 30 October 2020 Aegean Sea tsunami: post-event field survey along Turkish coast. Pure and Applied Geophysics. doi: 10.1007/s00024-021-02693-3

Elias P, Ganas A, Briole P, Valkaniotis S, Escartin J et al. (2021) Co-seismic deformation, field observations and seismic fault model of the Oct. 30, 2020 Mw = 7.0 Samos earthquake, Aegean Sea, EGU General Assembly 2021, online, 19–30 Apr 2021, EGU21-14595, https://doi.org/10.5194/egusphere-egu21-14595, 2021.

Elitez İ, Yaltırak C (2014). Burdur-Fethiye Shear Zone (Eastern Mediterranean, SW Turkey). In: EGU General Assembly 2014, Vienne, Austria.

Emre Ö, Duman TY, Özalp S, Şaroğlu F, Olgun Ş et al. (2018). Active fault database of Turkey. Bulletin of Earthquake Engineering 16 (8): 3229-3275. doi: 10.1007/s10518-016-0041-2

Ergin K, Güçlü U, Uz Z (1967). A catalogue of earthquakes of Turkey and surrounding area (11 A.D. to 1964 A.D.). İstanbul, Turkey: Maden Fakültesi Arz Fiziği Enstitüsü Yayınları.

Evelpidou N, Karkani A, Kampolis I (2021). Relative sea level changes and morphotectonic implications triggered by the Samos Earthquake of 30th October 2020. Journal of Marine Science and Engineering 9: 40. doi: 10.3390/jmse9010040

Eytemiz C, Erdeniz Ö F (2020). Investigation of active tectonics of Edremit Gulf, Western Anatolia (Turkey), using high-resolution multi-channel marine seismic data. Marine Science and Technology Bulletin 9 (1): 51-57. doi: 10.33714/masteb.635468

Havazlı E, Özener H. 2021. Investigation of strain accumulation along Tuzla fault - western Turkey. Turkish Journal of Earth Sciences 30:449-459

Eyübagil EE, Solak Hİ, Kavak US, Tiryakioğlu İ, Sözbilir H et al. (2021). Present-day strike-slip deformation within the southern part of İzmir Balıkesir Transfer Zone based on GNSS data and implications for seismic hazard assessment, western Anatolia. Turkish Journal of Earth Science 30: 143-160.

Fletcher R (1987). Practical Methods of Optimization. 2nd ed. New York, NY, USA: John Wiley & Sons.

Ganas A, Elias P, Briole P, Tsironi V, Valkaniotis S (2020). Fault responsible for Samos earthquake identified, Temblor. doi: 10.32858/temblor.134

Guidoboni, E, Comastri A, Traina G (1994). Catalogue of ancient earthquakes in the Mediterranean area up to the 10th century. Istituto Nazionale di Geofisica, Rome: 504 pp.

Guidoboni E, Comastri A, Boschi E (2005). The "exceptional" earthquake of 3 January 1117 in the Verona area (northern Italy): A critical time review and detection of two lost earthquakes (lower Germany and Tuscany). Journal of Geophysical Research: Solid Earth 110 (B12). doi: 10.1029/2005JB003683

Gülal E, Erdoğan H, Tiryakioğlu İ (2013). Research on the stability analysis of GNSS reference stations network by time series analysis. Digital Signal Processing 23: 1945-1957. doi: 10.1016/j.dsp.2013.06.014

Herring TA, King RW, Floyd MA, McClusky SC (2015). GAMIT Reference Manual, http://wwwgpsg.mit.edu/~simon/gtgk/GAMIT_Ref.pdf

Herring TA, King RW, Floyd MA, McClusky SC (2015). Introduction to GAMIT/ GLOBK, http://wwwgpsg.mit.edu/~simon/gtgk/Intro_GG.pdf

ISC (International Seismological center) (2020). Recent Earthquakes in Turkey [online]. Website http:// http://www.isc.ac.uk/ [accessed 4 November 2020].

Jackson J, McKenzie D (1984). Active tectonics of the Alpine–Himalayan Belt between western Turkey and Pakistan. Geophysical Journal of the Royal Astronomical Society 77 (1): 185-264. doi: 10.1111/j.1365-246X.1984.tb01931.x

Kirkpatrick S, Gelatt CD, Vecchi MP (1983). Optimization by Simulated Annealing Science 220: 671–680. doi: 10.1126/science.220.4598.671

Kürçer A, Özalp S, Özdemir E, Güldoğan ÇU, Duman TY (2019). Active tectonic and paleoseismologic characteristics of the Yenice-Gönen fault, NW Turkey, in light of the 18 March 1953 Yenice-Gönen Earthquake (Ms = 7.2). Bulletin of the Mineral Research and Exploration 159: 29-62. doi: 10.19111/bulletinofmre.500553

Le Pichon X, Chamot-Rooke N, Lallemant S, Noomen R, Veis G (1995). Geodetic determination of the kinematics of central Greece with respect to Europe: impli-cations for eastern Mediterranean tectonics. Journal of Geophysical Research Atmospheres 100 (12): 675–690. doi: 10.1029/95JB0031.7

Lisowski M (1997). Postseismic strain following the 1989 Loma Prieta earthquake from GPS and leveling measurements. Journal of Geophysical Research 102: 4933–4955.

Lykousis V, Anagnostou C, Pavlakis P, Rousakis G, Alexandri M (1995). Quaternary sedimentary history and neotectonic evolution of the eastern part of the Central Aegean Sea, Greece, Marine Geology 128: 59-71. doi: 10.1016/0025-3227(95)00088-G

Mascle J, Martin L (1990). Shallow structure and recent evolution of the Aegean Sea: asynthesis based on continuous reflection profiles. Marine Geology 94 (4): 271–299. doi: 10.1016/0025-3227(90)90060-W

McClusky S, Balasdsanian S, Barka A, Demir C, Georgiev I et al. (2000). Global positioning system constraints on crustal movements and deformations in the eastern Mediterranean and Caucasus. Journal of Geophysical Research 105 (B3): 5695–5719. doi: 10.1029/1999JB900351

McKenzie DP (1972). Active tectonics of the Mediterranean region. Geophysical Journal of the Royal Astronomical Society 30: 109–185.

McKenzie DP (1978). Active tectonics of the Alpine–Himalayan belt: the Aegean Sea and surrounding regions. Geophysical Journal of the Royal Astronomical Society 55 (1): 217-254. doi: 10.1111/j.1365-246X.1978.tb04759.x.

Mozafari N, Tikhomirov D, Sumer Ö, Özkaymak Ç, Uzel B et al. (2019). Dating of active normal fault scarps in the Büyük Menderes Graben (western Anatolia) and its implications for seismic history. Quaternary Science Reviews 220: 111-123. doi: 10.1016/j.quascirev.2019.07.002

Ocakoğlu N, Demirbağ E, Kuşçu İ (2004). Neotectonic structures in the area offshore of Alacati, Doganbey and Kusadasi (Western Turkey): evidence of strike-slip faulting in the Aegean extensional province. Tectonophysics 391 (1-4): 67–83. doi: 10.1016/j.tecto.2004.07.008

Okada Y (1985). Surface deformation to shear and tensile faults in a halfspace. Bulletin of the Seismological Society of America 75 (4): 1135–1154.

Özener H, Doğru A, Acar M (2013). Determination of the displacements along the Tuzla fault (Aegean region-Turkey): Preliminary results from GPS and precise leveling techniques. Journal of Geodynamics 67: 13-20. doi: 10.1016/j.jog.2012.06.001

Özkaymak Ç, Sözbilir H (2008). Stratigraphic and structural evidence for fault reactivation: The active Manisa fault zone, Western Anatolia. Turkish Journal of Earth Sciences 17 (3): 615-635.

Özkaymak C, Sozbilir H, Uzel B (2013). Neogene-Quaternary evolution of the Manisa basin: Evidence for variation in the stress pattern of the İzmir-Balıkesir Transfer Zone, Western Anatolia. Journal of Geodynamics 65: 117–135. doi: 10.1016/j.jog.2012.06.004

Papadimitriou P, Kapetanidis V, Karakonstantis A, Spingos I, Kassaras I et al. (2020). First Results on the Mw=6.9 Samos Earthquake of 30 October 2020. Bulletin of the Geological Society of Greece 56 (1): 251-279. doi: 10.12681/bgsg.25359

Papanikolaou D, Alexandri M, Nomikou P, Ballas D (2002). Morphotectonic structure of the western part of the North Aegean Basin based on swath bathymetry. Marine Geology 190: 465–492. doi: 10.1016/S0025-3227(02)00359-6

Papazachos BC, Comninakis PE (1971). Geophysical and tectonic features of the Aegean Arc. Journal of Geophysical Research 76 (35): 8517-8533. doi: 10.1029/ JB076i035p08517

Reilinger R, McClusky S, Vernant P, Lawrence S, Ergintav S et al. (2006). GPS constraints on continental deformation in the Africa-Arabia-Eurasia continental collision zone and implications for the dynamics of plate interactions, Journal of Geophysical Research Atmospheres 111 (B5): B05411. doi: 10.1029/2005JB004051

Papazachos BC, Papazachou CB (1997). The earthquakes of Greece. Ziti Publishing, Grecee, Thessaloniki: pp 304.

Pavlides S, Tsapanos T, Zouros N, Sboras S, Koravos G et al. (2009). Using Active Fault Data for Assessing Seismic Hazard: A Case Study from NE Aegean Sea, Greece. In: Earthquake Geotechnical Engineering Satellite Conference XVIIth International Conference on Soil Mechanics & Geotechnical Engineering; Alexandria, Egypt. pp 1-14.

Pınar N, Lahn E (1952). Türkiye depremleri izahlı kataloğu. Bayındırlık Bakanlığı Yapı ve İmar İşleri Reisliği Yayınları, Türkiye: 36 (6) (in Turkish).

Reddy CD, Sunil PS (2008). Post-seismic crustal deformation and strain rate in Bhuj region, western India, after the 2001 January 26 earthquake. Geophysical Journal International 172 (2): 593–606. doi: 10.1111/j.1365-246X.2007.03641.x

Reilinger R, McClusky S, Paradissis D, Ergintav S, Vernant P (2010). Geodetic constraints on the tectonic evolution of the Aegean region and strain accumulation along the Hellenic subduction zone. Tectonophysics 488 (1): 22–30. doi: 10.1016/j.tecto.2009.05.027

Sboras S, Pavlides S, Riccardo Caputo, Chatzipetros A, Michailidou A et al. (2011). Improving the resolution of seismic hazard estimates for critical facilities: the Database of Greek crustal seismogenic sources in the frame of the SHARE project. In: 30° Convegno Nazionale di Gruppo Nazionale di Geofisica della Terra Solida.

Soysal H, Sipahioğlu S, Kolçak D, Altınok Y (1981). Türkiye ve Çevresinin Tarihsel Deprem Kataloğu (2100 B.C.–1900 A.D.). TÜBİTAK, Rapor No: TBAG-341 (in Turkish).

Sözbilir H, Uzel B, Sumer O, Inci U, Yalcin-Ersoy E et al. (2008). Evidence for a kinematically linked EW trending İzmir Fault and NE-trending Seferihisar Fault: kinematic and paleoseismogical studies carried out on active faults forming the İzmir Bay, Western Anatolia. Geological Bulletin of Turkey 51 (2): 91-114.

Sözbilir H, Sümer Ö, Uzel B, Ersoy Y, Erkül F et al. (2009). The Seismic geomorphology of the Sığacık Gulf (İzmir) earthquakes of October 17 to 20, 2005 and their relationships with the stress field of their Western Anatolian region. Geological Bulletin of Turkey 52 (2): 217-238.

Sözbilir H, Sarı B, Uzel B, Sümer Ö, Akkiraz S (2011). Tectonic implications of transtensional supradetachment basin development in an extension-parallel transfer zone: the Kocaçay Basin, Western Anatolia. Turkey. Basin Research 23 (4): 423–448. doi: 10.1111/j.1365-2117.2010.00496.x

Sözbilir H, Sümer Ö, Uzel B, Eski S, Tepe Ç et al. (2017). 12 Haziran 2017 Midilli Depremi (Karaburun Açıkları) ve Bölgenin Depremselliği. Dokuz Eylül Üniversitesi Deprem Araştırma ve Uygulama Merkezi Raporu, 14s, http://daum.deu.edu.tr/?page_id=111&lang=tr

Sözbilir H, Tatar O, Akgün M, Ankaya P, Oya B et al. (2020). 30 Ekim 2020 Sisam (Samos) Depremi (mw: 6,9) Değerlendirme Raporu. doi: 10.13140/RG.2.2.33392.48644

Stucchi M, Rovida A, Capera AG, Alexandre P, Camelbeeck T et al. (2013). The SHARE European Earthquake Catalogue (SHEEC) 1000–1899. Journal of Seismology 17 (2): 523-544. doi: 10.1007/s10950-012-9335-2

Sümer Ö (2015). Evidence for the reactivation of a pre-existing zone of weakness and its contributions to the evolution of the Küçük Menderes Graben: a study on the Ephesus Fault, Western Anatolia, Turkey, Geodinamica Acta 27 (2-3): 130-154.

Tan O, Tapırdamaz MC, Yörük A (2008). The earthquake catalogues for Turkey. Turkish Journal of Earth Sciences 17 (2): 405-418.

Tan O, Papadimitriou EE, Pabuçcu Z, Karakostas V, Yörük A et al. (2014). A detailed analysis of microseismicity in Samos and Kusadasi (Eastern Aegean Sea) areas. Acta Geophysica. 62 (6): 1283-1309. doi: 10.2478/s11600-013-0194-1

Taxeidis K (2003). Study of historical seismicity of the Eastern Aegean Islands. PhD, National and Kapodistrian University of Athens, Athens, Greece (in Greek).

Taymaz T, Jackson J, McKenzie D (1991). Active tectonics of Alpine–Himalayan Belt between western Turkey and Pakistan. Geophysical Journal Research Astronomy Society 77: 185–265 doi: 10.1111/j.1365-246X.1984.tb01931.x

Tiryakioğlu İ, Floyd M, Erdoğan S, Gülal E, Ergintav S et al. (2013). GPS constraints on active deformation in the Isparta Angle region of SW Turkey. Geophysical Journal International 195 (3): 1455-1463. doi: 10.1093/gji/ggt323

Tiryakioğlu İ (2015). Geodetic aspects of the 19 May 2011 Simav earthquake in Turkey. Geomatics, Natural Hazards and Risk 6 (1): 76-89. doi: 10.1080/19475705.2013.831379

Tiryakioğlu İ, Baybura T, Özkaymak Ç, Sözbilir H, Sandıkçıoğlu A et al. (2015). Sultandağı Fayı Batı Kısmı Fay Aktivitelerinin Multidisipliner Çalışmalarla Belirlenmesi. Harita Teknolojileri Elektronik Dergisi 7 (1): 7-16 (In Turkish). doi: 10.15659/hartek.15.01.60

Tiryakioğlu İ, Yavaşoğlu H, Uğur MA, Özkaymak Ç, Yılmaz M et al. (2017a). Analysis of October 23 (Mw 7.2) and November 9 (Mw 5.6), 2011 Van Earthquakes Using Long-Term GNSS Time Series. Earth Sciences Research Journal 21 (3): 147-156. doi: 10.15446/esrj.v21n3.62812

Tiryakioğlu İ, Yiğit CÖ, Yavaşoğlu H, Saka MH, Alkan RM (2017b). The determination of interseismic, coseismic and postseismic deformations caused by the Gökçeada-Samothraki earthquake (2014, Mw = 6.9) based on GNSS data. Journal of African Earth Sciences 133: 86-94. doi: 10.1016/j.jafrearsci.2017.05.012

Tiryakioğlu İ, Aktuğ B, Yiğit CÖ, Yavaşoğlu HH, Sözbilir H et al. (2018a). Slip distribution and source parameters of the 20 July 2017 Bodrum-Kos earthquake (Mw6.6) from GPS observations. Geodinamica Acta 30 (1): 1-14. doi: 10.1080/09853111.2017.1408264

Tiryakioğlu İ, Uğur MA, Özkaymak Ç (2018b). Determination of Surface Deformations with Global Navigation Satellite System Time Series. Journal of Geological and Environmental Engineering 12 (11). doi: 10.5281/zenodo.2022043

Tiryakioğlu İ, Yiğit CÖ, Baybura T, Yılmaz M, Uğur MA et al. (2019). Active surface deformations detected by precise levelling surveys in the Afyon-Akşehir Graben, Western Anatolia, Turkey. Geofizika 36: 34-51. doi: 10.15233/gfz.2019.36.4

Tur H, Yaltırak C, Elitez İ, Sarıkavak KT (2015). Pliocene–Quaternary tectonic evolution of the Gulf of Gökova, southwest Turkey. Tectonophysics 638: 158–176. doi: 10.1016/j.tecto.2014.11.008

Vernant P, Reilinger R, McClusky S (2014). Geodetic evidence for low coupling on the Hellenic subduction plate interface. Earth and Planetary Science Letters 385: 122-129. doi: 10.1016/j.epsl.2013.10.018

Wang L, Wang R, Roth F, Enescu B, Hainzl S et al. (2009). Afterslip and viscoelastic relaxation following the 1999 M 7.4 Izmit earthquake from GPS measurements. Geophysical Journal International 178 (3): 1220–1237.

Wessel P, Luis JF, Uieda L, Scharroo R, Wobbe F et.al. (2019). The Generic Mapping Tools version 6. Geochemistry, Geophysics, Geosystems 20: 5556–5564. doi: 10.1029/2019GC008515

Yaltırak C (2002). Tectonic evolution of the Marmara Sea and its surroundings. Marine Geology 190: 493–530. doi: 10.1016/S0025-3227(02)00360-2

Yaltırak C, İşler EB, Aksu AE, Hiscott RN (2012). Evolution of the Bababurnu Basin and shelf of the Biga Peninsula: western extension of the middle strand of the Northeast Aegean Sea, Turkey. Journal of Asian Earth Sciences 57: 103–119. doi: 10.1016/j.jseaes.2012.06.016